One-dimensional Bi_2O_3 nanohooks: synthesis, characterization and optical properties

2007 J. Phys.: Condens. Matter 19 406204

(http://iopscience.iop.org/0953-8984/19/40/406204)

IOP PUBLISHING JOURNAL OF PHYSICS: CONDENSED MATTER

J. Phys.: Condens. Matter **19** (2007) 406204 (11pp) doi:10.1088/0953-8984/19/40/406204

One-dimensional Bi_2O_3 nanohooks: synthesis, characterization and optical properties

Latha Kumari, Jin-Han Lin and Yuan-Ron Ma[1]

Department of Physics, National Dong Hwa University, Hualien 974, Taiwan, Republic of China

E-mail: ronma@mail.ndhu.edu.tw

Received 4 April 2007, in final form 21 August 2007
Published 11 September 2007
Online at stacks.iop.org/JPhysCM/19/406204

Abstract

We report the synthesis of one-dimensional (1D) Bi_2O_3 nanohooks by the oxidative metal vapor phase deposition technique. Surface morphology observations confirm the formation of 1D nanohooks with nanoparticles at their tips. Structural analysis by x-ray diffraction (XRD) and transmission electron microscopy (TEM) reveals the crystalline nature of the 1D nanostructure. Elemental analysis confirms that the 1D nanohooks consist of only elements Bi and O. The XRD study suggests that the synthesized product is of two phases (α- and β-Bi_2O_3) with monoclinic and tetragonal crystal structures respectively. The phonon vibration modes corresponding to Bi_2O_3 are determined by Raman scattering. A broadband visible photoluminescence (PL) is observed in the wavelength region 500–900 nm, also indicating the extension of luminescence into the near-infrared region. The existence of broadband visible emission can be attributed to the existence of defect/impurity states induced by oxygen vacancies.

1. Introduction

One-dimensional (1D) metal oxide nanostructures such as wires, rods, tubes, belts, cables, ribbons, sheets and diskettes have become the focus of extensive research owing to their various outstanding properties (tunable physical properties) and unique applications in mesoscopic physics and fabrication of nanoscale devices in recent years [1, 2]. It is generally accepted that 1D nanostructures provide a good system to investigate the dependence of electrical, thermal transport and mechanical properties on dimensionality and size reduction (or quantum confinement). Oxides are the basis of smart and functional materials.

Bismuth oxide (Bi_2O_3) is an interesting material and very important in modern solid-state technology. It is fascinating to scientists owing to its unique structures and physical properties, such as a large energy band gap, high refractive index, dielectric permittivity and high oxygen-ion conductivity, as well as marked photoconductivity and photoluminescence (PL) [3–7].

[1] Author to whom any correspondence should be addressed.

These special features of Bi_2O_3 make it suitable for a large range of applications, such as sensors, optical coatings, photovoltaic cells and microwave integrated circuits [8–11]. These features explain the great effort devoted to the investigation of Bi_2O_3 polymorphs over the past few years.

Bi_2O_3 has five polymorphic forms that are denoted by α-Bi_2O_3 (monoclinic), β-Bi_2O_3 (tetragonal), γ-Bi_2O_3 (body centred cubic), δ-Bi_2O_3 (cubic), and ω-Bi_2O_3 (triclinic) [12, 13]. Among them, the low-temperature α-phase and the high-temperature δ-phases are stable, but the others are high-temperature metastable phases [14]. The tetragonal β-Bi_2O_3, which has a distorted defect-fluorite structure, is a metastable phase at ambient conditions and usually transforms into the stable monoclinic α-Bi_2O_3 at about 870 K. Each polymorph possesses distinct crystalline structures and physical properties (electrical, optical, mechanical, etc).

In spite of the scientific and technological importance of Bi_2O_3, the synthesis of the 1D nanostructures of Bi_2O_3 has not received great attention. To the best of our knowledge, very few reports on the synthesis of the 1D Bi_2O_3 nanostructures have appeared. Its successful synthesis can bring new features to existing useful materials. For the synthesis of oxide nanostructures, thermal evaporation of oxide powders is the most common method used [2]. Bismuth oxide nanostructures have been prepared using various techniques such as metal-organic chemical vapor deposition (MOCVD) [15], chemical method [16], oxidative metal vapor transport deposition technique [17], and simply oxidizing the Bi nanotube arrays by heat treatment method [18, 19]. As is known, the only study on the synthesis of the 1D Bi_2O_3 nanowires with thermal oxidation was reported by Yongfu *et al*, [17] but the synthesis procedure was quite different from the present work. In this paper, we describe a simple thermal oxidation method to synthesize the 1D Bi_2O_3 hook-like nanowires or simply nanohooks on the planar substrate at low temperature. The investigation of the surface morphology, the structure and the optical properties of the nanohooks is also presented.

2. Experimental details

The synthesis of the 1D Bi_2O_3 nanohooks was carried out by an oxidative metal vapor phase deposition technique. First, the Bi granules were placed in a carbon holder and the holder was mounted on the heater, externally adjusted by a temperature controller. A p-type Si(100) wafer was ultrasonically cleaned with acetone, ethyl alcohol and deionized water in sequence each for 30 min and was placed over the carbon holder at a height of $\sim$3 mm to facilitate the sample deposition. At the base pressure of about 10^{-3} Torr, argon flow of 180 sccm was introduced into the chamber and the working pressure was maintained at 10 Torr throughout the synthesis process for obtaining the specified nanostructures. After obtaining the constant working pressure, the current in the temperature controller was adjusted to obtain a sufficient temperature for melting and evaporating the Bi granules. The temperature required to melt and vaporize the Bi effectively in order to obtain the expected nanostructures, was optimized by repeated trials. Oxygen (O_2) of 0.6 sccm was introduced into the chamber for about 30 s in the beginning and then twice for 5 s after intervals of 10 min. In the last 10 min O_2 was not fed into the chamber; however the growth process continued with the existing O_2 pressure inside the chamber. The time taken for the whole synthesis process was 30 min. The temperature of the substrate was found to be below $\sim$350 °C. After cooling down to room temperature, a sufficiently thick layer of light yellow colored product was found on the Si substrate. The advantage of this approach is the easy control of the nanostructures' growth via the adjustment of the heater temperature and other working parameters.

Surface morphology analysis was performed on the 1D nanostructures by a field emission scanning electron microscope (FESEM, JEOL JSM-6500F) with energy-dispersive

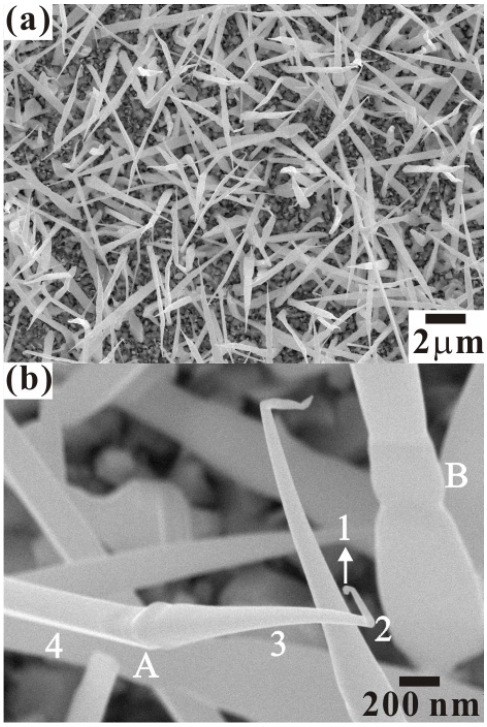

Figure 1. Low-magnification (a) and high-magnification (b) FESEM images of the 1D Bi_2O_3 nanohooks. The four distinct regions of the single 1D nanohook are marked as 1, 2, 3 and 4 respectively. A and B represent the two joints of the 1D nanohooks.

x-ray spectroscopy (EDS) installed and was operated at an accelerating voltage of 15 kV. Transmission electron microscopy (TEM) images and selected area electron diffraction (SAED) patterns were obtained from the apparatus JEOL-3010, employing an accelerating voltage of 200 kV. For TEM analysis, the nanohook product were ultrasonically dispersed in ethanol and then dispersed on the carbon-coated copper grids. Structural analysis was carried out by employing an x-ray diffractometer (Philips X'Pert) with Cu Kα radiation ($\lambda = 1.5406$ Å). A micro-Raman spectrometer (Jobin Yvon Horiba T64000) with 532 nm incident photons from a diode-pump-solid-state laser at a maximum power of 50 mW, equipped with a liquid-nitrogen-cooled charge-coupled device (CCD) detector was employed to obtain Raman scattering spectra. Photoluminescence of these nanostructures were studied with a scanning near-field optical microscope (Alpha SNOM 300 series) with excitation laser of 488 nm (MELLES GRIOT 43 series ion laser).

3. Results and discussion

3.1. Surface morphology

Figure 1 represents FESEM images of the 1D Bi_2O_3 nanohooks. A dense and uniform deposition of the 1D Bi_2O_3 nanohooks on the Si(100) surface is observed in figure 1(a). At the beginning of the growth process, Bi_2O_3 nanoparticles are deposited on the Si surface, which later assist the growth of the Bi_2O_3 nanohooks [17]. These nanohooks are randomly arranged, indicating that the growth direction of the nanostructure is randomized. Figure 1(b) shows the

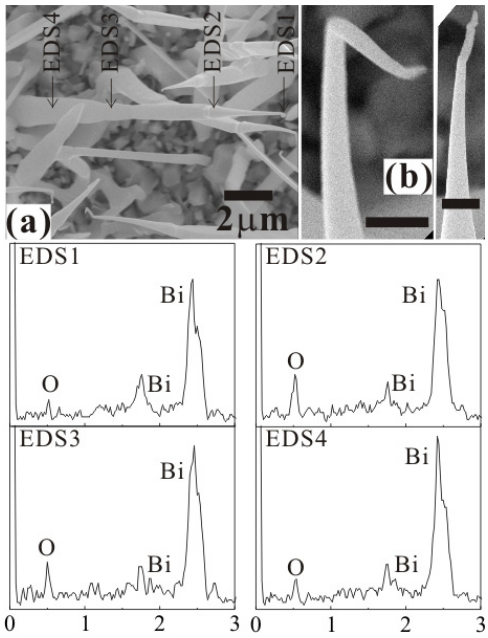

Figure 2. FESEM images of the 1D Bi_2O_3 nanohooks: (a) image indicating the four different regions, (b) high-magnification images showing the single hook-like and finger-like nanostructures respectively (scale bar 200 nm). EDS1–4 are EDS spectra of four different regions of the 1D nanohook marked respectively in (a).

high-magnification FESEM image of 1D nanohooks. The growth of each nanohook has four distinct regions: the nanoparticle of about 20–100 nm diameter at its tip (marked as 1), then the hook-like nanostructure (marked as 2), followed by a cone-like structure (marked as 3) and later the nanowire-like growth of uniform diameter (marked as 4). These 1D nanohooks show two joints, one between the cone-like and nanowire-like region (marked as A), and the other between the two nanowire-like regions of different widths (marked as B), as shown in figure 1(b).

An FESEM image in figure 2(a) shows a single nanohook indicating four distinct regions accordingly marked with arrows, at which the EDS measurement was performed. The two high-magnification FESEM images of the 1D nanohook (figure 2(b)) present the growth of two kinds of 1D nanostructure, one with a hook-like structure and the other with a finger-like structure. No specific conditions can be accounted for the formation of different 1D nanostructures. The EDS spectra of the 1D nanohook at four distinct regions were obtained as shown in figure 2(a), and are represented as EDS1, EDS2, EDS3 and EDS4. The EDS spectra indicate that these 1D nanostructures consist of only the elements Bi and O, regardless of the position on the nanohook and they have the ratio of O to Bi approximately equal to 3:2. The atomic concentration % of O to Bi corresponding to the EDS1–EDS4 plots are 63.23:36.77; 64.75:35.25; 64.16:35.84 and 63.23:36.77 respectively. The present observation confirms that both the nanoparticle and nanowire have the same elemental composition forming Bi_2O_3, unlike the previous study [17] where the spherical nanoparticle was composed of almost 100% Bi.

The thickness of the yellow colored product (1D Bi_2O_3 nanostructure) formed on the Si substrate was approximately 3 μm. The FESEM was operated at an accelerating voltage of 15 kV, which is expected to effectively probe deep into the sample, as it depicts the increase in interaction volume. The penetration depth of the beam depends directly on the accelerating

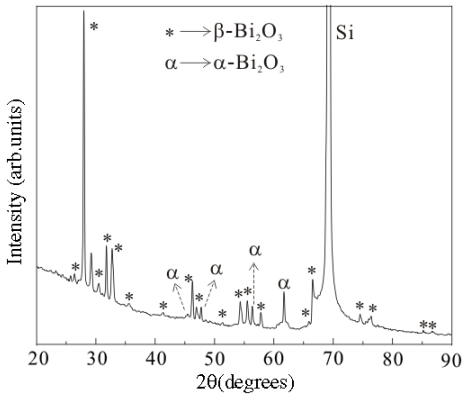

Figure 3. XRD profile of the 1D Bi_2O_3 nanohooks representing a two-phase system with diffraction peaks corresponding to β-Bi_2O_3 (*) and α-Bi_2O_3 (α).

voltage and is supposed to be greater in low density specimens [20]. The theoretical depth of penetration of an 'average' electron into bismuth calculated using the electron range equation [20, 21] is about 1 μm at 15 kV. Hence, bismuth oxide, being less dense than bismuth, is supposed to account for the better penetration depth ($\sim$1–2 μm). However, in practice, approximately 5% of the signal collected by a secondary electron (SE) detector is composed of back-scattered electrons (BSEs). In theory, increasing the accelerating voltage up to a maximum of approximately 16 kV will result in increased depth from which BSEs are detected for high atomic number specimens, up to a maximum of approximately 6 μm. Hence, at a higher accelerating voltage, the information obtained regarding the specimen is more from BSEs than SEs. Indeed, BSEs are emitted from deeper within the sample, allowing more information to be gained with respect to nano-features, underlying thicker areas of the specimen. This is compared to SEs which provide information regarding the surface topography of a specimen with characteristic energy below 50 eV and emerge from within 20 nm of a surface [22]. Hence, a higher accelerating voltage provides better depth probing with moderate resolution.

3.2. Structural analysis

Figure 3 displays a typical XRD profile of the 1D Bi_2O_3 nanohooks. Most of the diffraction peaks in the spectra are indexed as β-Bi_2O_3 (tetragonal) with lattice constants, $a = 0.7742$ nm and $c = 0.5631$ nm (indicated by '*') and are in agreement with those of the standard data (JCPDS 78-1793) [17, 18]. However, the XRD spectrum also shows four prominent diffraction peaks (indicated by 'α') corresponding to the presence of small traces of α-Bi_2O_3 (monoclinic) with lattice constants, $a = 0.585$ nm, $b = 0.817$, $c = 0.751$ and $\beta = 112.98°$ (JCPDS 41-1449) [15]. These diffractions peaks are indexed to $(\bar{2}31)$, (140), $(\bar{2}42)$, and $(\bar{3}33)$ planes. Hence, the XRD results confirm that the as synthesized 1D Bi_2O_3 nanohooks have mixed Bi_2O_3 phases (α- and β-Bi_2O_3) with monoclinic and tetragonal crystal structures respectively. The strong diffraction peak at around 27.94° corresponding to (201) indicates that the 1D Bi_2O_3 nanohooks have a preferential orientation along the (201) direction pertaining to tetragonal β-Bi_2O_3 [17, 18]. A strong peak around 69° which arises due to the substrate effect is attributed to the Si(004) plane.

Further, the structural information of the single nanohook is also displayed in the TEM images, SAED pattern and the corresponding EDS spectrum. Figure 4(a) shows the three TEM

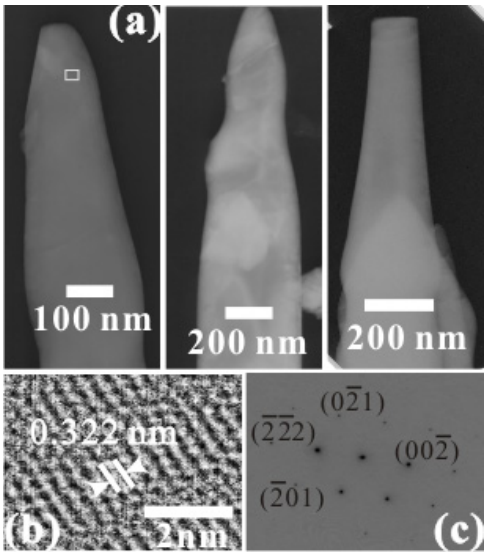

Figure 4. (a) TEM images of the three single 1D Bi_2O_3 nanohooks, (b) HRTEM image, and (c) SAED pattern corresponding to the area marked with a box in (a).

images of the single 1D nanohook of width about 160–440 nm. The visible lattice fringes of the high-resolution TEM (HRTEM) image recorded near the edge of the 1D nanowire region (indicated by a box) is shown in figure 4(c). From the image, clear lattice fringes are observed, indicating that the 1D nanowire is of a single crystalline nature. These fringes are separated by 0.322 nm, which agrees with the interplanar spacing corresponding to the (201) plane. The growth direction of the 1D nanohook follows along the (101) direction. The SAED pattern (figure 4(d)), with the incident electron beam parallel to the (010) direction and perpendicular to the long axis of the nanohook is acquired. The reflections in the SAED pattern correspond to the lattice planes of bulk Bi_2O_3, indicating that the 1D material is crystalline, as is also confirmed from XRD analysis.

3.3. Raman scattering

Raman spectroscopy is a powerful and nondestructive experimental technique for probing the vibrational and structural properties of materials. It allows easy discrimination between various compositions and structures. It is recognized as a powerful tool to identify different polymorphs of metal oxides. It is well known that α-Bi_2O_3 and β-Bi_2O_3 have Raman features in the 50–600 cm^{-1} range while γ-Bi_2O_3 and δ-Bi_2O_3 have their Raman bands in 50–900 cm^{-1} range and the Raman data for the ω-Bi_2O_3 have yet to be reported. In accordance with the instrument access limit, the Raman bands recorded above 60 cm^{-1} are reported in the present work. The Raman peaks due to the heavy metal oxides such as Bi_2O_3, may be classified into four main sets [23] denoted as: (1) low wavenumber Raman modes (30–70 cm^{-1}), (2) heavy metal ion vibrations in the range 70–160 cm^{-1}, (3) bridged anion modes in the intermediate 300–600 cm^{-1} region, and (4) nonbridging anion modes at higher wavenumbers. Our Raman spectrum (figure 5) shows peaks associated to the (2) and (3) categories of vibrations that supports the network forming character of Bi.

Figure 5 shows the Raman scattering spectrum of the 1D Bi_2O_3 nanohooks, obtained in ambient atmosphere with an excitation wavelength of 532 nm, which contains a low frequency

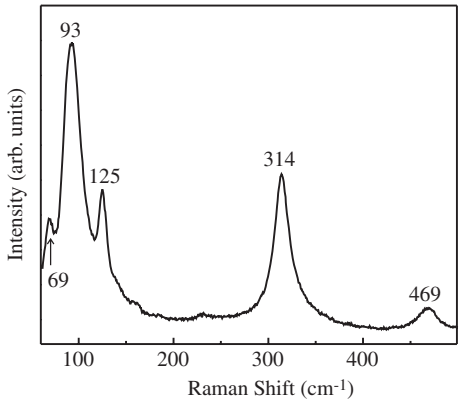

Figure 5. Raman scattering spectrum of the 1D Bi_2O_3 nanohook with the corresponding Raman bands marked.

region ranging from 60 to 500 cm^{-1}. In the region below 120 cm^{-1}, the Raman peaks are attributed to vibration modes of heavy elements such as bismuth or lattice vibrations, and above 150 cm^{-1}, the Raman bands can be attributed to oxygen vibrations. The modes in the range 120–150 cm^{-1} are defined by the displacements of both Bi and O atoms [24]. The molecular structure of the bismuth oxide polyhedra in β-Bi_2O_3 is proposed to be BiO_6 octahedra with all Bi–O bonds equivalent at 2.40 Å. The bismuth oxide polyhedron in β-Bi_2O_3 has a molecular structure similar to that found in α-Bi_2O_3 [25].

The Raman spectrum of the 1D Bi_2O_3 nanohooks in figure 5 shows five prominent Raman bands at 69, 93, 125, 314 and 469 cm^{-1}. The two first-order Raman modes at 69 and 93 cm^{-1} are assigned respectively to the E_g and A_{1g} vibration modes of Bi in Bi_2O_3 [24–27]. However, the Raman band corresponding to the E_g mode is very weak compared to the A_{1g} mode. The three Raman bands observed at 125, 314 and 469 cm^{-1} are expected to be due to three unique Bi–O stretches [25]. These Raman bands are attributed to the β-Bi_2O_3 (tetragonal) phase [25, 27]. However, the appearance of peaks at 69 and 93 cm^{-1} in the Bi_2O_3 system can also be assigned to the presence of traces of α-Bi_2O_3 [24, 27] as evident in XRD studies (figure 3). From figure 5. It is evident that the oxygen modes show broad bands in comparison with the bismuth modes, which provides evidence for the strong anharmonicity of the oxygen modes [24].

3.4. Photoluminescence

Bismuth ions (Bi^{3+}, Bi^{2+}) have been used as a luminescent activator and also as a sensitizer in various host materials in the past [28–32]. First, Bi^{3+} ions can directly absorb incident electromagnetic radiation. The optical properties of crystals activated by Bi^{3+} ions are attributed, as a rule, to the electron transitions between the states $6s^2$ and 6s6p in the trivalent ion of bismuth. The ground state of the bismuth ion is totally symmetric ($^1S_0$). The excited levels corresponding to the configuration 6s6p are the triplet levels $^3P_0$, $^3P_1$, and $^3P_2$ and the singlet level $^1P_1$. All the selection rules allow only the transition $^2S_0$–$^1P_1$. The transition $^1S_0$–$^3P_2$ is forbidden by the selection rule for the total momentum of the atom J. The transition $^1S_0$–$^3P_1$ is allowed owing to the spin–orbital interaction of the $^3P_1$ and $^1P_1$ states. The transitions $^1S_0$–$^3P_1$ and $^1S_0$–$^1P_1$, the first of which is longer-wave, are realized in the bands of optical absorption and excitation of the photoluminescence of bismuth-activated substances. The energy position

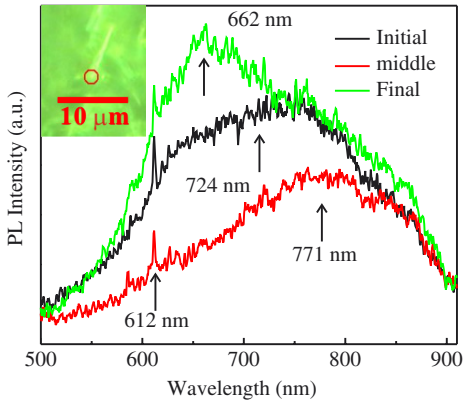

Figure 6. Photoluminescence spectra of the single 1D Bi_2O_3 nanohook recorded at three different areas. The inset shows the CCD image of the single nanohook. The region marked with a red circle represents the initial point.

(This figure is in colour only in the electronic version)

of these bands, just as the position of the luminescence bands (from the UV region of the spectrum to the red), strongly depends on the type of matrix. The common property of bismuth-activated crystals is the presence of wide-band luminescence, which, as a consequence of nonradiative transitions, is attributed to the lowest-frequency allowed transition $^3P_1$–$^1S_0$. Secondly, the charge-transfer transition from the O^{2-} ion to the empty 6p level of the Bi^{3+} ion is possible. Generally the former is known to occur easily in many cases [30]. Furthermore, the luminescence of Bi ions usually appears in the visible wavelength region. However, the luminescent properties of pure bismuth and Bi_2O_3 are seldom reported. There are two main reasons for the luminescence of Bi_2O_3 nanostructures: the quantum size effect and structural defects in the crystals [33].

Figure 6 represents the PL spectrum of the single 1D Bi_2O_3 nanohook. The PL spectra were recorded on three different regions of the 1D nanohook: the hook-like region (initial), the joint of cone-like and nanowire-like structure (middle) and the nanowire-like region (final), shown respectively in the CCD image (inset of figure 6). The PL spectra corresponding to different nanostructures show broadband emission wavelengths in the range, 500–900 nm (visible to near-infrared region) which can be attributed to defects or impurity-trapped emissions [28, 32]. The values of peak maxima for three different regions of the nanohook are 724, 771 and 662 nm respectively and the corresponding full width at half maximum (FWHM) values are 265, 198 and 345 nm. A sharp peak observed at 612 nm in the PL spectra for the three different regions of Bi_2O_3 nanohook can also be attributed to defect states. Moreover, the PL spectra in figure 6 also show weak and broad shoulders at around 630 and 830 nm for all three regions. However, non-monotonic variations in peak maxima and FWHM are observed for different regions of the nanohook which may arise due to the varying morphology and size of the nanostructures.

Broadened emission and the emission maxima between 660–770 nm are observed in the PL spectrum. Such low-energy emission is attributed to the crystal defects or defect levels associated with oxygen vacancies or bismuth interstitials that have formed during growth. During the Bi_2O_3 nanostructure synthesis, a high density of oxygen vacancies and Bi vacancies was expected. The oxygen vacancies, which may mainly lie on the surface of the nanostructures, interact with interfacial bismuth vacancies and lead to formation of a

considerable number of trapped states within the bandgap; this results in a greater PL intensity at room temperature [34]. Regarding the shift of the peak position (first to longer wavelength region, then to shorter wavelength region), we suppose that it may be caused by the residual stresses within the Bi_2O_3 nanostructures, which originate from the lattice distortion. In fact, the contrast observed in the TEM images (figure 4) confirms the presence of strain (stresses) within the nanostructures. The shifting of the emission band to a shorter wavelength region is sometimes also attributed to the quantum size effects in the nanostructures [33].

In general, the emission of a Bi ion is assigned to its electrovalency, which arises from different S–P transitions [28]. Furthermore, the visible emission band arises from an energy transfer among Bi^{3+} ions (internal transitions of Bi^{3+} ions). The β-Bi_2O_3 nanotube arrays are also indicated by the PL broad emission band (excitation wavelength, 291 nm) [19]. Visible photoluminescence observed in thermally annealed Bi implanted SiO_2 films [32] depicts broadband emission in the wavelength region, 500–800 nm (excitation wavelength of 488 nm) with a peak maximum at 590 nm (2.1 eV). The origin of the 2.1 eV PL band is speculated to be the Bi cluster which has a discrete electronic level formed by the non-metallic band. Our recent study [35] of PL in 1D Bi_2O_3 nanowires shows a spectrum with visible broadband emission, in the wavelength region of 500–800 nm with peak maximum at 589 nm. A small peak was also observed at 528 nm, which was attributed to the green emission corresponding to the Bi^{3+} ions. In the present work, the broadband emission extends from the visible to the near-infrared region. However, the emission band maximum lies in the vicinity of visible region, unless in some bismuth-doped glasses [29, 31, 36, 37] which observed the luminescence band maximum in the infrared region. Even the FWHMs for the emission bands in Bi_2O_3 nanohooks are large and comparable with these materials. If the infrared luminescence is expected to come from the Bi_2O_3 nanostructures, it should not be arising from the direct transitions from conduction band to valence band since the band gap energy of Bi_2O_3 is about 3.3 eV [3]. It might be from recombinations between the defect levels in the band gap or from the defect levels to the valence band [29]. From previous studies [29, 31, 36, 37], it is evident that the infrared emission is not due to either Bi^{3+} or Bi^{2+} ions. Hence, it is speculated that the origin of infrared emission may be Bi^{+}, unstable Bi^{5+} ions or bismuth clusters [29, 31, 36, 37]. However, there is no evidence proving this until now and therefore a more detailed study is required. It was found that the peak wavelength, shape and spectral width of the emission band could be controlled drastically by the excitation wavelength [29, 31, 36, 37]. This suggests a possible extension of PL into the deep infrared region, by increasing the excitation wavelength, to explore the application of Bi_2O_3 nanostructures as broadband optical fiber amplifiers and tunable lasers [29, 31, 36, 37].

3.5. Growth mechanism

The present synthesis technique of the Bi_2O_3 nanostructures can be termed as a self-catalyzed vapor–liquid–solid (VLS) mechanism [38] coupled with oxidation reaction. In our experiment, since no catalytic metals are used, the growth of the nanostructures is expected to be governed by a vapor–solid process [39], in which the vapor originates from the starting materials in a high temperature zone and thereby facilitates the formation of one-dimensional nanostructures in a low temperature zone. The deposition parameters such as evaporation temperature, Ar flow rate, oxygen flow rate, working pressure and position of substrate above the carbon holder were found to play significant roles in the synthesis of the Bi_2O_3 nanostructures and hence, are optimized to obtain the uniform formation of 1D nanostructures reported in this paper. At the higher O_2 concentrations, the Bi droplets are excessively oxidized to Bi_2O_3 which severely reduces the self-catalytic role of Bi. Initially, the high concentration of O_2 is sufficient for Bi_2O_3 nucleation and the subsequent lower concentrations can sustain the nanostructure growth. The

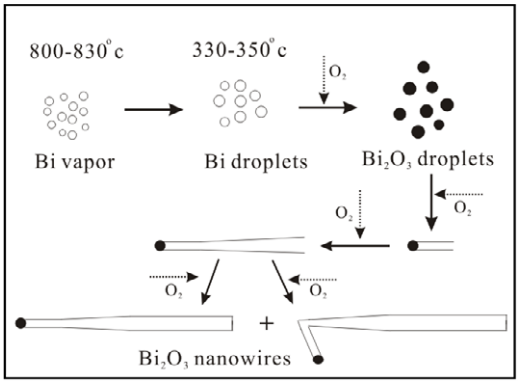

Figure 7. Schematic illustrating the growth mechanism of the 1D hook-like Bi_2O_3 nanowires, or nanohooks.

method of oxygen injection followed in the present work has proven to be very effective for the synthesis of Bi_2O_3 nanostructures.

Figure 7 represents a schematic diagram showing the growth mechanism of the 1D Bi_2O_3 hook-like nanowires or nanohooks. First, the Bi vapor is generated at high temperature (800–830 °C), followed by the Bi vapor transfer to the low temperature zone by the assistance of Ar flow. During the synthesis process, the evaporation temperature is very important to obtain a sufficiently high Bi vapor pressure. The high Ar flow rate allows quick transfer of the Bi vapor to the lower temperature zone. The low temperature region condenses the Bi vapor to form little Bi droplets. When O_2 is introduced into the chamber, the O_2 diffuses into the low-temperature region and reacts with the Bi droplets to form Bi_2O_3 nanoclusters. As the O_2 concentration decreases to a certain level, the nucleation of the Bi_2O_3 is suppressed and the growth of the 1D Bi_2O_3 nanostructures takes place only at the interface of the Bi_2O_3 nuclei and the Bi_2O_3 droplets, leading to the elongation of the Bi_2O_3 phase. Under suitable conditions, a steady state is established between the Bi vapor, Bi droplet, O_2 gas, and the Bi_2O_3 phases, which supports the smooth and controlled growth of the 1D nanostructure [17].

Hence, the periodic injection of O_2 is expected to play a significant role in the formation of different structures in the 1D nanohooks. This method of synthesis of the 1D hook-like nanowire structures is quite different from the conventional VLS mechanism [38] where a foreign metal catalyst is used for directing the nanostructure growth. In our case, Bi metal is used as both a source and a catalyst. A self-catalyzed VLS process with controlled injection of O_2 is proposed to be responsible for nucleation and a vapor–solid (VS) process for the 1D nanostructure growth [40]. The nanostructure growth technique discussed in this work can be effectively used in the preparation of many other metal oxide nanostructures.

4. Conclusions

1D Bi_2O_3 nanohooks were synthesized by the oxidative metal vapor phase deposition technique. The structural analysis by XRD, HRTEM and SAED confirms the crystalline nature of the 1D Bi_2O_3 nanohooks. The Raman bands of the 1D Bi_2O_3 nanohooks below 120 cm^{-1} are assigned to vibration mode of Bi and above 120 cm^{-1} are attributed to the oxygen vibrations in Bi_2O_3. The PL spectra of the 1D nanohooks show visible to infrared broadband emission (500–900 nm), which can be attributed to defect/impurity states induced by oxygen vacancies present in the Bi_2O_3 nanostructures. In addition, these nanostructures may

be applied to broadband optical fiber amplifiers and tunable lasers. This work also presents the simple and novel synthesis procedure for the formation of a new kind of nanostructure, the 1D Bi_2O_3 nanohooks. The synthesis technique of 1D Bi_2O_3 nanohooks is termed a self-catalyzed, reaction-coupled VLS mechanism, without the use of a foreign catalyst, which can be employed for the production of various nanostructures by controlling the synthesis parameters.

Acknowledgments

We are grateful to the National Science Council of the Republic of China for financially supporting this research under contract Nos. NSC 95-2112-M-259-013-MY2 and NSC 95-2811-M-259-001.

References

[1] Xia Y, Yang P, Sun Y, Wu Y, Mayers B, Gates B, Yin Y, Kim F and Yan H 2003 *Adv. Mater.* **15** 353
[2] Dai Z R, Pan Z W and Wang Z L 2003 *Adv. Funct. Mater.* **13** 9
[3] Leontie L, Caraman M, Alexe M and Harnagea C 2002 *Surf. Sci.* **507** 480
[4] Fruth V, Popa M, Berger D, Ramer R, Gartner M, Ciulei A and Zaharescu M 2005 *J. Eur. Ceram. Soc.* **25** 2171
[5] Fan H T, Teng X M, Pan S S, Ye C, Li G H and Zhang L D 2005 *Appl. Phys. Lett.* **87** 231916
[6] Thayer R L, Randall C A and Trolier-McKinstry S 2003 *J. Appl. Phys.* **94** 1941
[7] Sammes N M, Tompsett G A, Nafe H and Aldinger F 1999 *J. Eur. Ceram. Soc.* **19** 1801
[8] Kanazawa E, Sakai G, Shimanoe K, Kanmura Y, Teraoka Y, Miura N and Yamazoe N 2001 *Sensors Actuators* B **77** 72
[9] Fu J 1997 *J. Mater. Sci. Lett.* **16** 1433
[10] George J, Pradeep B and Joseph K S 1987 *Phys. Status Solidi* a **100** 513
[11] Chopra K L and Das S R 1983 *Thin Film Solar Cells* (New York: Plenum)
[12] Blower S K and Greaves C 1998 *Acta Crystallogr.* C **44** 587
[13] Gualtieri A F, Immovilli S and Prudenziati M 1997 *Powder Diffract.* **12** 90
[14] Shuk P, Wiemhöfer H-D, Guth U, Göpel W and Greenblatt M 1996 *Solid State Ion.* **89** 179
[15] Kim H W, Myung J H and Shim S H 2006 *Solid State Commun.* **137** 196
[16] Gujar T P, Shinde V R, Lokhande C D and Han S-H 2006 *Mater. Sci. Eng.* B **133** 177
[17] Qiu Y, Liu D, Yang J and Yang S 2006 *Adv. Mater.* **18** 2604
[18] Li L, Yang Y-W, Li G-H and Zhang L D 2006 *Small* **2** 548
[19] Yang B, Mo M, Hu H, Li C, Yang X, Li Q and Qian Y 2004 *Eur. J. Inorg. Chem.* **2004** 1785
[20] Richards R G, Wieland M and Textor M 2000 *J. Microsc.* **199** 115
[21] Kanaya K and Okayama S 1972 *J. Phys. D: Appl. Phys.* **5** 43
[22] Wood M A, Meredith D O, Owen G Rh, Richards R G and Riehle M O 2005 *Nanotechnology* **16** 1433
[23] Kharlamov A A, Almeida R M and Heo J 1996 *J. Non-Cryst. Solids* **202** 233
[24] Denisov V N, Ivlev A N, Lipin A S, Mavrin B N and Orlov V G 1997 *J. Phys.: Condens. Matter* **9** 4967
[25] Hardcastle F D and Wachs I E 1992 *J. Solid State Chem.* **97** 319
[26] Onari S, Miura M and Matsuishi K 2002 *Appl. Surf. Sci.* **197/198** 615
[27] Salazar-Pérez A J, Camacho-López M A, Morales-Luckie R A, Sánchez-Mendieta V, Ureña-Núñez F and Arenas-Alatorre J 2005 *Superficies y Vacío* **18** 4
[28] Blasse G 1994 *J. Phys. Chem. Solids* **55** 171
[29] Peng M, Wang C, Chen D, Qiu J, Jiang X and Zhu C 2005 *J. Non-Cryst. Solids* **351** 2388
[30] Bordun O M 2002 *J. Appl. Spectrosc.* **69** 67
[31] Meng X, Qiu J, Peng M, Chen D, Zhao Q, Jiang X and Zhu C 2005 *Opt. Express* **13** 1635
[32] Komatsu M, Oyoshi K, Hishita S, Matsuishi K, Onari S and Arai T 1998 *Mater. Chem. Phys.* **54** 286
[33] Dong W and Zhu C 2003 *J. Phys. Chem. Solids* **64** 265
[34] Hu J, Bando Y, Liu Q and Goldberg D 2003 *Adv. Funct. Mater.* **13** 493
[35] Kumari L, Lin J-H and Ma Y-R 2007 *Nanotechnology* **18** 295605
[36] Suzuki T and Ohishi Y 2006 *Appl. Phys. Lett.* **88** 191912
[37] Denker B, Galagan B, Osiko V, Sverchkov S and Dianov E 2007 *Appl. Phys.* B **87** 135
[38] Wagner R S and Ellis W C 1964 *Appl. Phys. Lett.* **4** 89
[39] Sears G W 1956 *Acta Metall.* **3** 268
[40] Kar S, Pal B N, Chaudhuri S and Chakravorty D 2006 *J. Phys. Chem.* B **110** 4605